RADAR CHARACTERISTICS OF SMALL CRATERS: IMPLICATIONS FOR VENUS

RONALD GREELEY[1,2], PHILIP R. CHRISTENSEN[1], and JOHN F. McHONE[1]

(Received 11 April, 1986)

Abstract. Shuttle radar images (SIR-A) of volcanic and impact craters were examined to assess their appearance on radar images. Radar characteristics were determined for: (a) 9 maarlike craters in the Pinacate volcanic field, Sonora, Mexico; (b) the caldera of Cerro Volcan Quemado, in the Bolivian Andes; (c) Talemzane impact crater, Algeria; and (d) Al Umchaimin, a possible impact structure in Iraq. SIR-A images were compared with conventional photographs and with results from field studies. Consideration was then given to radar images available for Venus, or anticipated from the Magellan mission. Of the criteria ordinarily used to identify impact craters, some can be assessed with radar images and others cannot be used; planimetric form – expressed as circularity – and ejecta-block distribution can be assessed on radar images, but rim and floor elevations relative to the surrounding plain and disposition of rim strata are difficult or impossible to determine. We conclude that it will be difficult to separate small impact craters from small volcanic craters on Venus using radar images, and suggest that it will be necessary to understand the geological setting of the areas containing in order to determine their origin.

1. Introduction

Solar System exploration frequently involves the return of images. Because of thick cloud cover, the surface of Venus remains hidden to all but radar imaging, supplemented by limited views from landed spacecraft. Pioneer Venus returned radar data, Earth-based radar has provided low-resolution coverage of much of Venus, and the Soviet Venera 15 and 16 orbiters have returned radar images of Venus; principally of the northern region. These spacecraft and the proposed U.S. Venus radar mapper (Magellan) promise to provide moderate-resolution (a few hundred meters to a few kilometers) images for much of Venus.

Among the features likely to be observed are craters that have formed by a variety of processes. Both volcanic and impact craters occur on all other inner planets and it is reasonable to expect them on Venus (Head and Wilson, 1985; Burns and Campbell, 1985). Size-frequency distributions of impact craters provide the primary means for dating planetary surfaces (Hartmann *et al.*, 1981). Craters ~ 2 to 20 km in diameter provide the best means for relative dating of planetary surfaces; larger craters are too scarce to provide statistically meaningful data except for very large areas, whereas smaller craters may have been partly mantled or modified by erosional processes, especially on planets that have atmospheres. The assumption is made that only impact craters are included in crater count analyses and that craters of other origins can be identified and isolated. Such identifications are usually based on

[1] Department of Geology.
[2] Center for Meteorite Studies, Arizona State University, Tempe, Ariz., U.S.A.

Earth, Moon, and Planets **37** (1987) 89–111.

morphological characteristics; however, this task is difficult in volcanic areas where endogenic craters occur (Greeley and Gault, 1979) or where erosional processes have modified the original crater morphology.

Numerous investigators have speculated on the presence of impact craters on Venus (Schaber and Boyce, 1977; Masursky *et al.*, 1980; Pettengill *et al.*, 1980; Campbell and Burns, 1980; Cutts *et al.*, 1981). Because of limited image resolution, most of these studies have involved examination of features $> \sim 20$ km. However, images of features in the size range appropriate for crater statistics are anticipated from both the Venera and the proposed Magellan missions. Preliminary analysis from the Venera 15 and 16 missions (Basilevsky, 1984) reveals numerous craters in this size range. However, these images and those from Earth-based radar also show various volcanic features, so it is likely that endogenic craters exist on Venus (Burns and Campbell, 1985; Head *et al.*, 1985).

The objective of this report is to describe radar characteristics of some volcanic craters and impact structures on Earth that were imaged by the Shuttle Imaging Radar (SIR-A) experiment and discuss the results in light of what may be imaged by Magellan. The SIR-A experiment was flown aboard the space shuttle Columbia in 1981 and produced images with spatial resolution of ~ 40 m (Settle and Taranik, 1982). The experiment involved a side-looking, synthetic aperture, horizontally polarized, microwave-radiation system transmitting and receiving an L-band frequency beam (23.5 cm wavelength) at an incidence angle of $50 \pm 3°$ from the vertical. The radar system on Magellan will also be a side-looking, synthetic-aperture, horizontally polarized system, but the beam will be in the S-band frequency (12.6 cm wavelength), and the incidence angle will vary between 15° and 44°. The spatial (ground) resolution of the Magellan images will be between 120 and 300 m in both the azimuth and range directions.

The percent of radar signal reflected back to the antenna from a surface is a function of the surface slope, dielectric constant, and surface roughness. The slope and dielectric constant control the amount of energy that is specularly reflected from the surface, while the roughness determines the degree and angular variability of the diffusely scattered component. For radar systems such as SIR-A and Magellan, the only energy that is specularly reflected back to the spacecraft comes from surface elements with diameters of approximately 1 to 1000 radar wavelengths (25 cm to 250 m for SIR-A, 13 cm to 125 m for Magellan) that are oriented normal to the radar beam and look direction (Tyler, 1971; Moore *et al.*, 1980). Thus, depending upon orientation, slopes and facets may produce strong radar returns, with the maximum return from slopes near $50 \pm 3°$ in the SIR-A observations, and from slopes between 15° and 44° (depending on the incidence angle) for Magellan. The dielectric constant of the surface also controls the amount of reflection from these slopes. For most geologic materials the dielectric constant varies by only a factor of 2 to 3 (Campbell and Ulrichs, 1969), but even a few percent moisture content within the surface can produce a factor of 10 or more increase in reflectivity (Hoekstra and Delaney, 1974). Thus, wet surfaces produce the strongest radar returns, if they are properly oriented.

Fig. 1. Oblique aerial view westward of MacDougal Crater, Pinacate volcanic field, Mexico, showing the prominent outer rim (a) and the inner rim (b). The crater floor is covered with alluvium and talus deposits and has a small central playa (dark zone); the crater is about 1.6 km across.

Diffuse reflection is produced by Rayleigh scattering from rocks and other roughness elements that are on the order of 1/2 wavelength or larger in size (Beckmann and Spizzichino, 1963). This energy is scattered nearly isotropically, so that a bright return is observed regardless of the surface orientation. In addition, the diffuse component is typically depolarized, while the specular component retains the polarization of the incident beam. Unfortunately, SIR-A did not permit multiple polarization observations, nor will Magellan, so the two components cannot be separated.

Four sites were analyzed in our study: (a) the Pinacate field, a volcanic-aeolian terrain in northern Mexico; (b) Cerro Volcan Quemado, a silicic volcano in the western Andes of Bolivia; (c) Talemzane impact crater, Algeria; and (d) Al Umchaimin, a possible impact structure in Iraq. Although most of these craters are at the smaller size limit for detection by current missions to Venus, this analysis

provides insight into the ability to discriminate craters of various origins and provides some basis for interpreting radar images returned from Venus. Additionally, most of these sites are located in arid regions, reducing the variability of the dielectric constant due to differing moisture contents.

2. Sites Investigated

2.1. Pinacate Volcanic Field, Mexico

The Pinacate volcanic field consists of a complex shield volcano, associated cinder cones, flows, and maar craters, all set in an arid terrain of fault-block mountains and sedimentary basins. Some flows and tephra deposits may be as young as 300 years. The field contains 9 craters (Table I), most of which are phreatic or phreatomagmatic features (maars) that have been enlarged by collapse (Jahns and Fielder, 1952; Jahns, 1959; Gutmann, 1976). Collapse during and following the explosive phase widened and deepened the craters. Most of the craters pierce sequences of older lava flows and cinder deposits, now exposed in the crater walls. The craters have topographically raised rims and tend to have flat floors, resulting from partial filling by sediments (Arvidson and Mutch, 1974). The degree of explosivity, collapse, and modification varies among the craters; some are moderately eroded or mantled by sediments, and others are relatively pristine. This affords the opportunity to assess the radar characteristics for a variety of volcanic crater morphologies and stages of degradation. Six examples of these craters are discussed below.

MacDougal Crater

MacDougal Crater, one of the largest craters at Pinacate, has pronounced inner and outer rims (Figure 1). As mapped by Jahns (1959), the outer rim exposes platy tuff deposits 20–50 m thick. The main cliff-forming units are vesicular basalt flows that are cut by steeply dipping dikes up to 4 m thick. The crater floor is mantled by yellow, sandy sediments and includes a small playa. A small reentrant in the southeast wall defines the head of a debris flow that spills onto the floor. Talus deposits are uniformly distributed around the rest of the wall-floor boundary and fans of talus extend onto the floor.

The radar image (Figure 2a) shows MacDougal Crater as a large, bright ring. This enhanced signal return is produced by the rim topography and roughness, rock ledges near the crest of the rim, and blocky talus on the wall. A radar shadow on the south wall is cast by the outer rim, indicating an inward-dipping slope steeper than $40 \pm 3°$. The floor is radar-dark, corresponding to the smooth, flat-lying alluvium, with lighter, radar-mottled spots in the central part surrounding a dark area. The mottled areas are most likely produced by diffuse return from the vegetation surrounding the small playa. The contact between the floor and the rim is radar-mottled, corresponding to shallow gullies, whereas the talus fans that extend onto the floor show as bright 'spikes' on the radar image. The reentrant in the crater wall and its associated debris flow show as a slight asymmetry in the crater rim. Outer flanks of

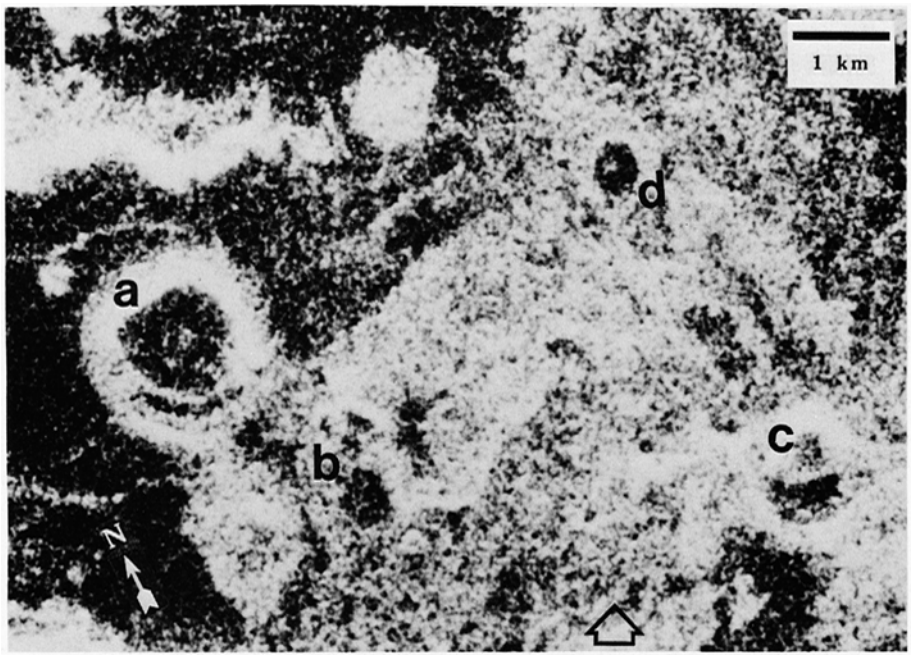

Fig. 2a. SIR-A image of part of the western Pinacate volcanic field showing MacDougal Crater (a), Molina Crater (b), Crater Grande (c), and Badillo Crater (d). Radar look direction is indicated by the large arrow.

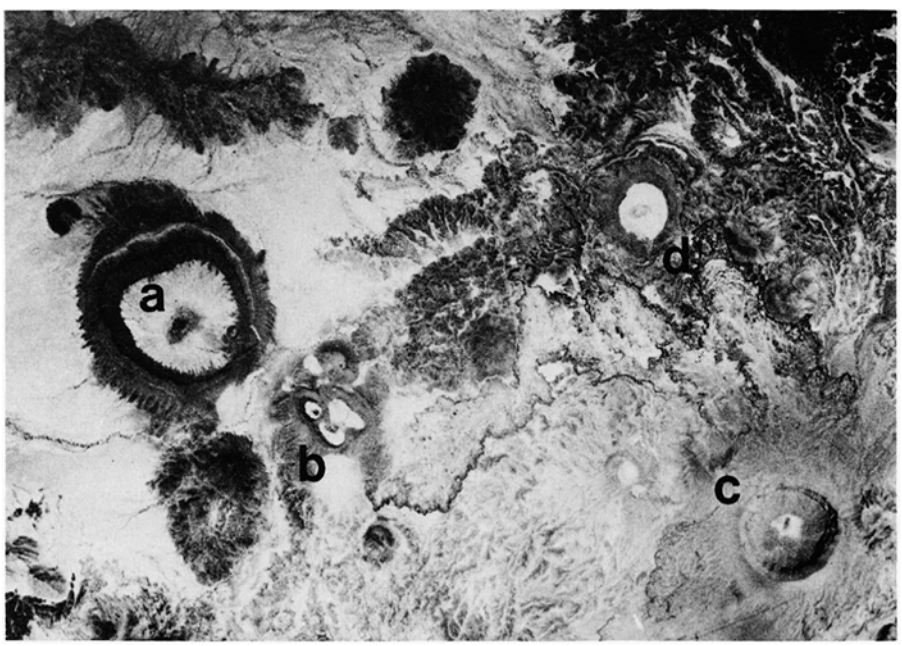

Fig. 2b. Aerial photograph corresponding to Pinacate volcanic field shown in Figure 2a; crater designations are the same.

Fig. 3. Oblique aerial view northeastward of Badillo Crater showing the flat, smooth floor, low rim deposits composed of tuff breccia, and a basalt ledge on the far crater wall; the crater is about 600 m across.

the crater are radar-dark mottled, corresponding to regions of sheetwash and gullying. The radar-dark zone on the west flank defines a smooth mantle of windblown sands derived from the Gran Desierto to the west.

Badillo Crater

This small crater is surrounded by a ring of tuff breccias that slope outward from the rim crest to form a gentle ramp and slope inward more steeply to the crater floor (Figures 2, 3). Basalt flows exposed by the crater crop out to form a small ledge on the northeast wall. Badillo cuts at least three older cinder cones which pre-date the crater (Jahns, 1959). In the radar image (Figure 2a), the floor of the crater is visible as a radar-dark ovoid surrounded by a bright ring set on a background of relatively radar-bright terrain. The bright ring results primarily from rim roughness, although basalt outcrops on the northern rim also contribute to the radar return. The crater

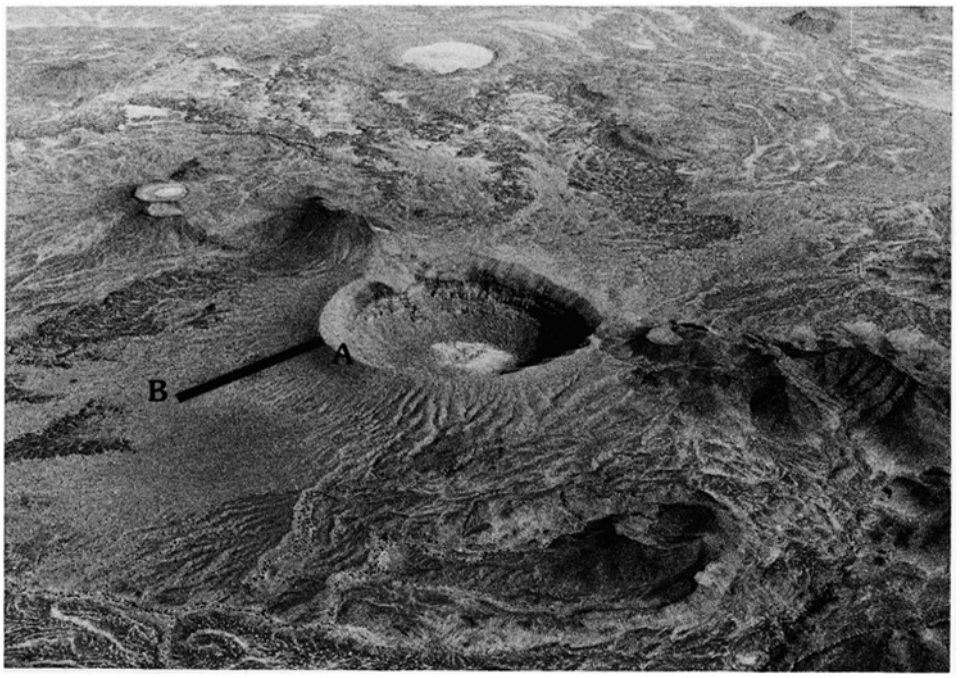

Fig. 4. Oblique aerial view northwestward of Crater Grande (middle foreground; 1 km across) and Crater Badillo (background). Line shows where traverse was made; station 0 is at A, station 70 at B.

floor is filled with alluvium and windblown sands, both of which are smooth and radar-dark. Off center on the crater floor is a zone of vegetation that is radar-bright. Outer flanks of the crater are indistinguishable from the surrounding terrain and rim slopes are too shallow to cast a radar shadow.

Crater Grande

The steep walls of this crater (Figure 4) expose two sequences of basalt flows, an upper unit composed of 1- to 3-m-thick flow units and a lower series of dense to vesicular basalt flows. Layers of cinders are found between some flow units. The rim is composed of 30 to 40 m of very coarse tuff breccias, some of which dip outward as much as 30–38°. On the north and northeast side, rim deposits rest on thick wedges of cinders which can be traced to a cone transected by the crater. The crater floor is covered by alluvium, talus, and playa deposits.

In the radar image (Figure 2), the crater rim and walls show as a bright ring and the steep wall casts a prominent radar shadow from the south side. The crater floor is radar-dark, corresponding to alluvial deposits. Crater Grande has the steepest ($\sim 28°$) outer flank slopes of the craters examined and displays a wide range of radar brightnesses. A traverse was made to assess the surface properties from the rim crest to a radar-dark region southwest of the crater (Figure 5). Several factors could contribute to the strong radar reflectivity: from the rim crest to ~ 120 m downslope,

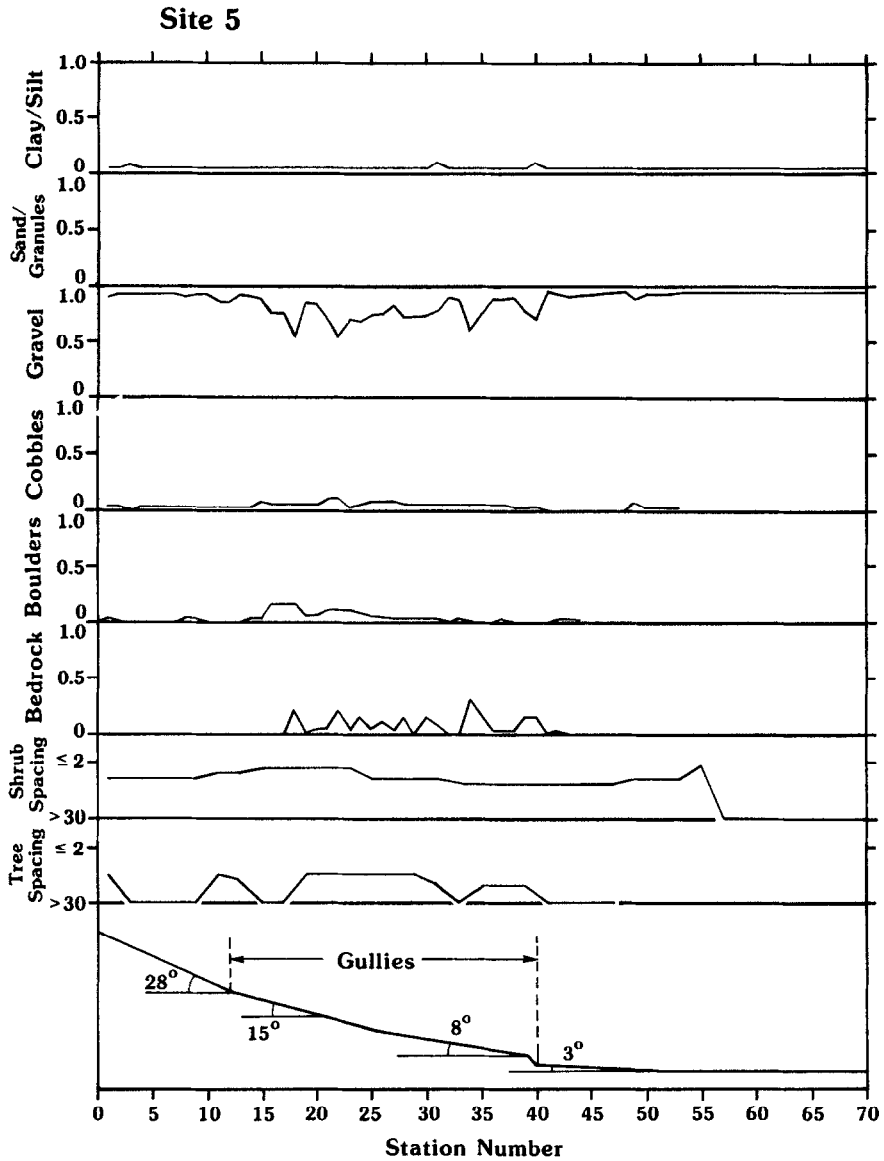

Fig. 5. Radial traverse southeast for 700 m across the south rim of Crater Grande showing the distributions of particle sizes and vegetation with respect to topography.

the surface is smooth and vegetation-free, but has a steep slope (~ 28°) oriented toward the radar beam. Where the slope decreases from 28° to 15° there is an increase in boulders (up to 15% areal coverage) and the beginning of a gullied zone which produce a strong radar return. Gullies are spaced 60–80 m apart, are as wide as 20 m and 6–8 m deep, and have wall slopes up to 32°. Numerous basaltic boulders and outcrops of indurated tuff deposits in the gullies produce strong radar backscattering.

Fig. 6. Oblique aerial view southward of Cerro Colorado showing the wide apron of alluvium on the outer flanks and the high crater rim on the southeast side of the crater (upper left side); crater rim diameter is about 1 km (ASU photograph 2329-D).

A second decrease in slope occurs 400 m from the rim crest. Gullies end, boulders and outcrops of tuff are no longer exposed, and the surface consists of silt and clay, gravels, and scattered patches of small cobbles. The abrupt change in surface properties at this point correlates with a sharp radar boundary between a strong return from the rim slope (radar-bright on the image) and a weak return from the flat-lying surface. Despite a wide variety of potential radar reflectors, there is little variation in radar return from the outer rim area. Thus, radar brightness can be a combination of factors; increases in surface roughness can offset decreases in slope and produce nearly constant radar returns.

Cerro Colorado

Cerro Colorado has cut through alluvium on the northeast margin of the volcanic field (Figure 6). The rim is asymmetric and is most prominent on the southeast side where it rises 110 m above the plains. The rim is composed of tuff breccias that consist of thinly layered ashes overlain by gravelly tuff with granitic and metamorphic rock fragments. Outer rim flanks are deeply gullied. The oldest rocks occur in the western wall and are composed of vesicular basalt overlain by gray tephra deposits. The crater floor consists of alluvium and playa deposits. The outer flank of the crater forms a broad apron of alluvium and weathered tuff breccias derived from the rim.

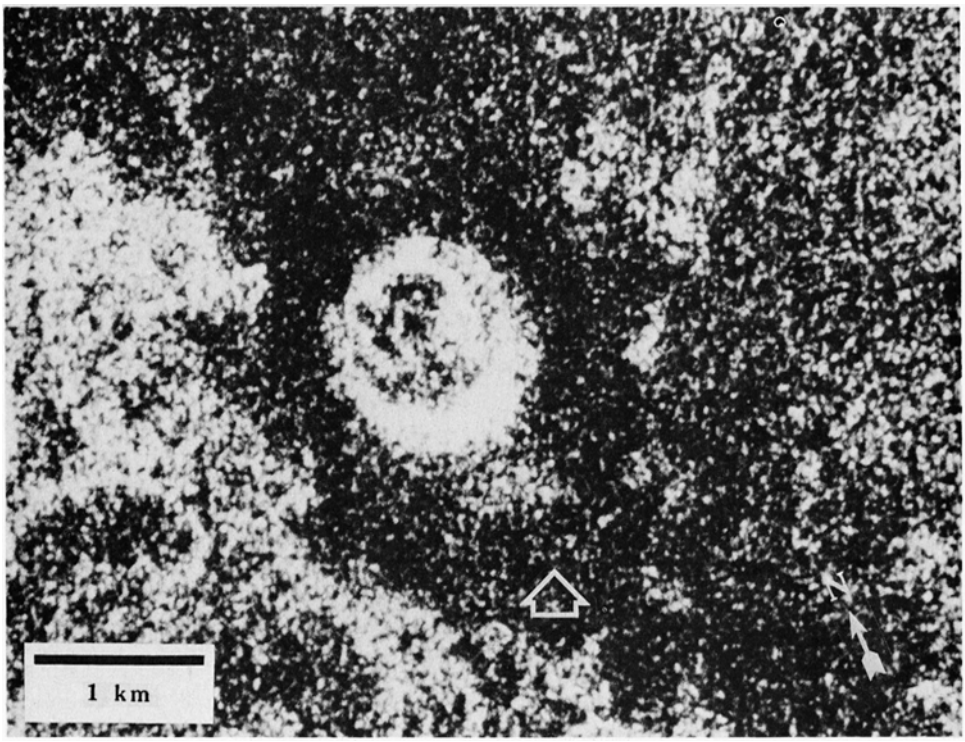

Fig. 7. Radar image of Cerro Colorado; look direction is shown by large arrow.

In the radar image (Figure 7), the rim is bright and shows the widening on the southeast side. A dark, curvilinear feature on the south side corresponds to the steepest part of the rim and could be a radar shadow. A thick ash deposit on the south side forms a steep slope facing the direction of radar illumination and contributes to the radar return. The gullied part of the rim shows on the radar image as faint radial streaks, particularly on the northeast and southwest sides where gullying is most prominent. The crater floor is mottled and shows a bright zone extending from the east side, corresponding to deposits of tuff breccia extending inward from the rim. In addition, a radar-bright zone appears to correspond to heavier vegetation. The most distinctive radar feature, an encircling radar-dark collar, corresponds to the wide apron of alluvium and weathered ash.

Elegante Crater

Elegante Crater is the largest and most complex crater in the Pinacate field (Figure 8) and has been studied extensively (Jahns, 1959; Gutmann, 1972; Wood, 1974; Donnelly, 1974; Gutmann and Sheridan, 1978; Lynch, 1981). This nearly circular crater pierces a series of cinder deposits and basalt flows to form steep walls. The rim consists of tuff breccias which average 50 m thick and dip as much as 30° away from the rim, although the average is only ~ 6°. Jahns (1959) proposed that a lake previously occupied the crater, and cited as evidence the delta deposits which form

Fig. 8. Oblique aerial view westward of Elegante Crater, showing smooth and gullied outer flanks of the crater and the reentrant in the rim on the left side; crater is about 1.3 km across (ASU photograph 240-A).

a distinct bench some 65 m above the floor. These deposits consist of mudstones, sandstones, and pebble conglomerates derived from the crater walls. The crater floor is covered by alluvium and playa sediments. Crater Elegante has the simplest rim of the craters observed; it is raised ~ 70 m above the surrounding plains, forms an unbroken inner slope of ~ 35°, and has a symmetric exterior slope.

In the radar image (Figure 9), the inner rim facing the radar beam is distinctly bright while a pronounced radar shadow is cast from the steep south rim. A reentrant on the east wall, barely discernable on the radar image, corresponds to a transected cinder cone. Radar-bright mottled areas on the southwest half of the floor correspond to delta deposits and talus. The northeastern floor of the crater is radar-dark, corresponding to alluvium and playa deposits. Outer flanks of the crater form a diffuse, radar-bright mottled zone, corresponding to gullies.

Moon Crater

Moon Crater is on the south-east side of the volcanic field and is being encroached by windblown sands (Figure 10). The crater rim is composed mostly of tuff breccias and the crater floor is covered with alluvium and aeolian sands. A small cone in the center is composed of basaltic spatter (Lynch, 1981) and post-dates the phreatic phase of crater formation. Moon crater appears as a radar-bright ring (Figure 11) and contrasts with radar-dark aeolian sediments to the southwest and radar-mottled

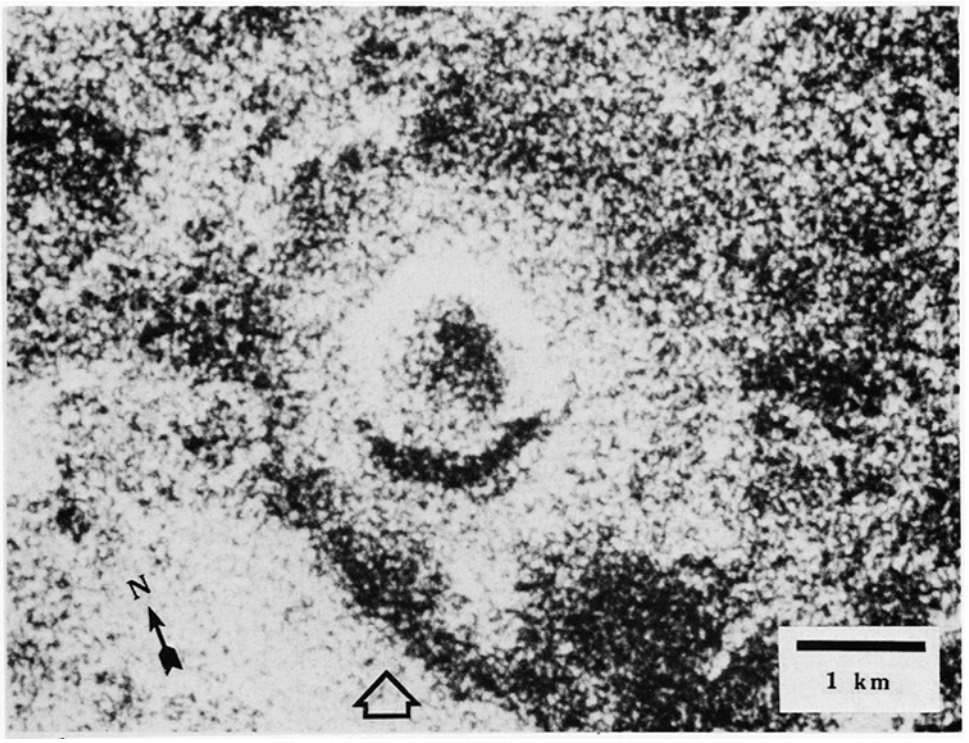

Fig. 9. SIR-A image of Elegante Crater showing a prominent radar shadow from the south rim and the bright diffuse collar generated by gullies on the crater flank; arrow shows look direction.

Fig. 10. High oblique aerial view northward of Moon Crater on the southwest edge of Pinacate volcanic field showing the low, rounded rim and the central spatter cone and crater on its floor; Moon Crater is about 300 m across (ASU photograph 2343-A).

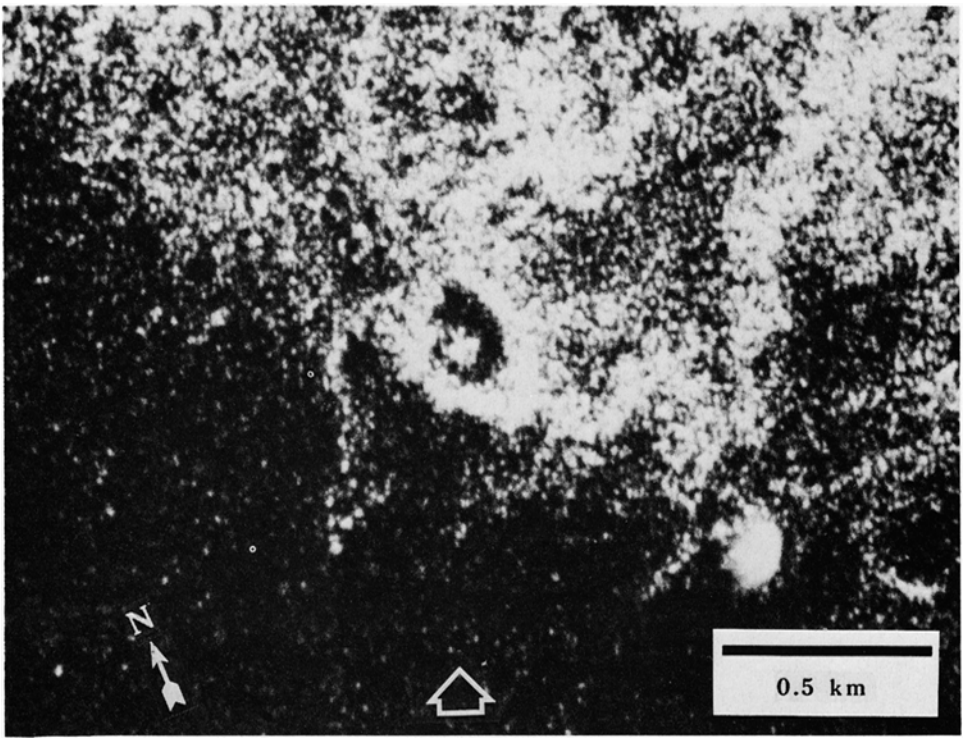

Fig. 11. Radar image of Moon Crater. Look direction indicated by arrow; radar-mottled pattern in upper right half of image corresponds to lava flows; radar-dark area in lower left is covered by windblown sand.

fine-grained alluvial sediments to the north and northeast. Radar brightness results primarily from rim roughness, although a small ledge of rock on the northeastern wall also contributes to the radar return. The crater floor is filled with windblown sediments and alluvium derived from the crater rim. Moderately-developed gullying contributes to radar mottling on the southwest side. The small spatter cone on the crater floor is visible as a radar-bright spot. However, the summit crater on the cone is not visible, despite its being more than half the diameter of the cone.

2.2. Cerro Volcan Quemado, Bolivia

Cerro Volcan Quemado (Figure 12a) is a volcano on the eastern edge of the Cordillera Occidental, the predominantly volcanic chain of the Andes (Ahlfeld, 1972). It is 6.5 km in diameter at the base and rises 350 m above the surrounding plain. The summit is marked by a caldera 2.1 by 3.4 km across, composed of a series of coaslescing craters as deep as ~ 75 m. The slope of the inner crater walls range from ~ 35° to nearly vertical. A prominent, blocky dome is located within the southernmost crater (Figure 13). Much of the volcano's flanks and the surrounding plains are covered by relatively fine-grained ash and pumice to a radial distance of ~ 7 km.

Fig. 12a. Vertical aerial photograph of Cerro Volcan Quemado, a silicic volcano with a prominent caldera and central dome in the Andes of Bolivia. Area shown is 6.7 km by 10.8 km; north is toward the top.

Fig. 12b. SIR-A image corresponding to Figure 12a. The bright area in the center corresponds to the blocky dome shown in Figure 13. Radar look direction is indicated by arrow.

Fig. 13. Oblique aerial view southward of Cerro Volcan Quemado showing the dome and block flow originating from center of the crater complex.

In the radar image (Figure 12) the caldera appears as an oval feature with bright scalloped segments corresponding to the coaslescing crater rims. Strong radar return appears to result primarily from steep slopes facing the spacecraft, but the roughness of the blocky dome and rock outcrops in the rims also contribute to the signal. A halo of fine material surrounding the summit craters produces a radar-dark mottled region.

2.3. Talemzane Crater, Algeria

Talemzane crater (Figure 14), located 400 km south-southeast of Algiers, Algeria, is 1.75 km in diameter and 70 m deep. First suggested by Karpoff (1954) and Brady (1954) as an impact structure, Talemzane crater was subsequently visited by Lambert *et al.* (1980), who provide definitive evidence for an impact origin. Talemzane formed in Eocene limestones; its raised rim is composed of strata which are, in places, vertical or overturned. A surrounding zone of uplifted strata extends 500 m

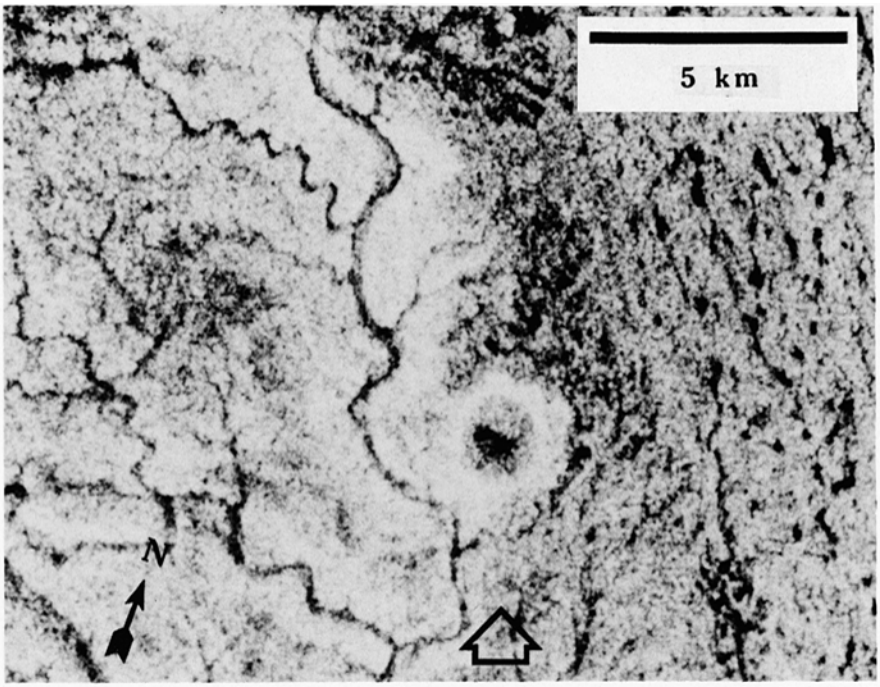

Fig. 14. SIR-A image of Talemzane Crater, Algeria. Arrow shows look direction.

from the rim crest. The crater walls are injected with breccia veins that are both parallel and perpendicular to the strata, and limestones in the crater wall are intensely fractured at a spacing of ~ 1 cm. Breccia also occurs at the base of the wall and consists of clasts up to 1 m across. The crater floor is covered with alluvium, whereas crater flanks expose ejecta deposits with angular to sub-rounded blocks. In general, block size decreases with distance from the rim; blocks 2 to 3 m across are common in the rim, although fragments as large as 5 to 10 m across are also found. The SIR-A image (Elachi *et al.*, 1982) shows a radar-bright ring surrounding a mottled zone and an offset radar-dark area. The bright ring corresponds to blocky ejecta that produce strong backscattering. The central dark zone corresponds to fine-grained alluvial sediments.

2.4. Al Umchaimin Crater, Iraq

Al Umchaimin crater (Figure 15a) lies 90 km west-southwest of Rutba in western Iraq. As described by Merriam and Holwerda (1957), this ~ 3.2 km diameter crater has a maximum depth of 35 m. Its rim is continuous and lies slightly above the surrounding Al Itanad plain, which has a maximum relief of several meters and is covered with a desert pavement of chert gravels. Interior crater walls consist of terraces 1 to 2 m high down to a depth of 10 to 15 m, below which are talus and alluvial fans extending 750 m onto the crater floor. Most of the crater floor is covered with playa deposits. The entire region is underlain by horizontal Eocene limestone

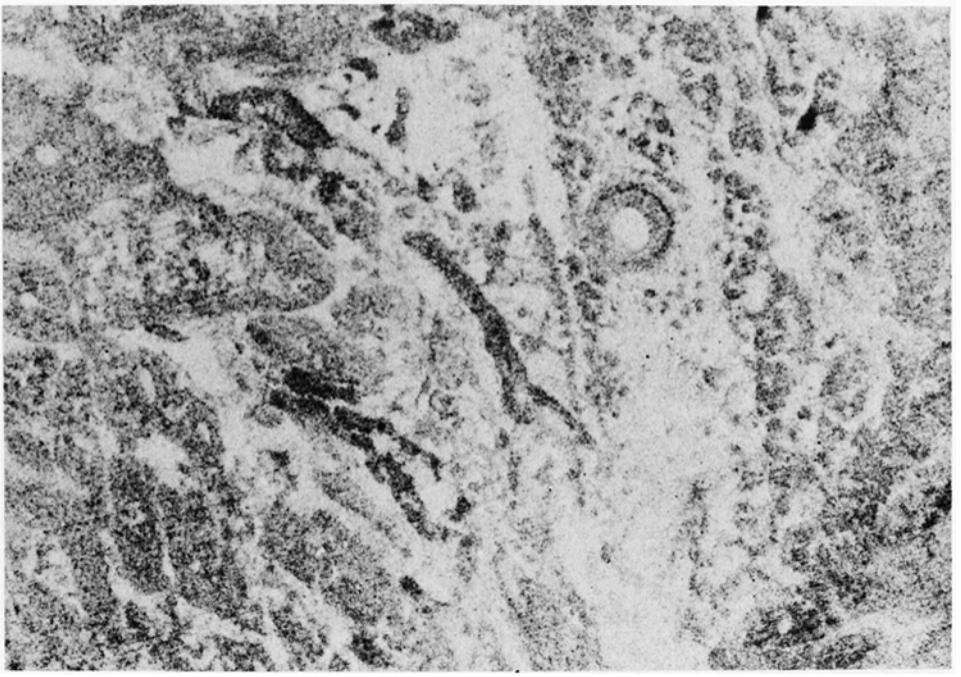

Fig. 15a. Landsat image of Al Umchaimin depression, Iraq. This structure, measuring 3.2 km across, shows rim structure suggestive of an impact origin. Area shown is 26 × 35 km.

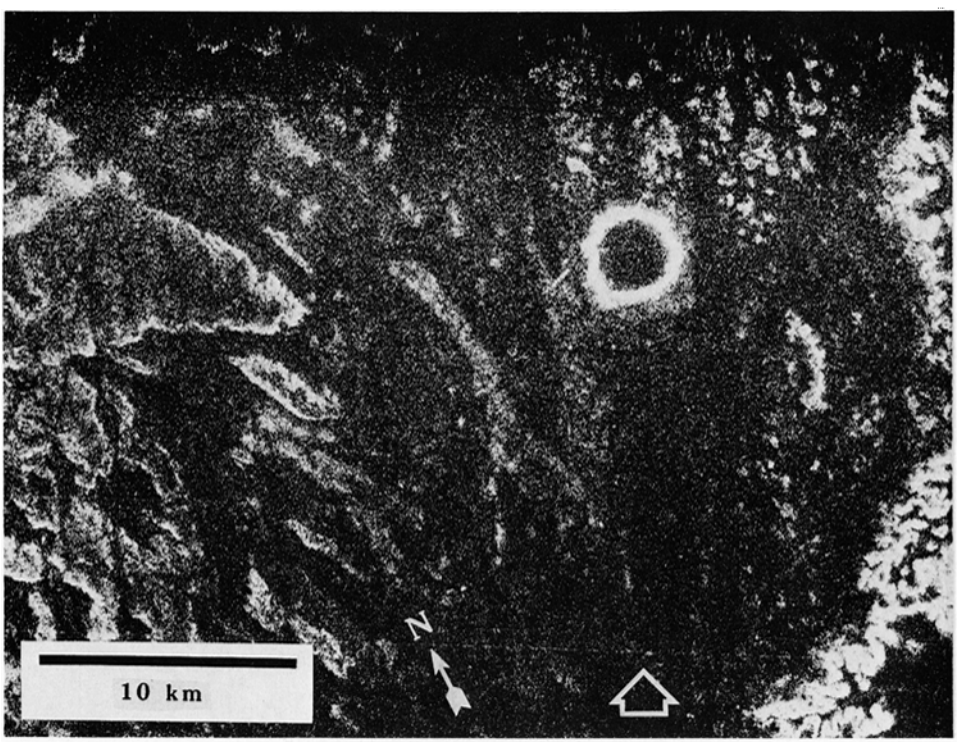

Fig. 15b. SIR-A image of Al Umchaimin depression. Radar look direction is shown by arrow.

beds. Although no definitive impact features have been reported, the circularity and slightly uplifted rims suggest an impact origin. The radar image shows an intense, bright ring corresponding to the crater rim. This strong return is due principally to blocky rubble on the rim slopes, as it does not vary with the radar-viewing angle as would be expected for slope-related signal return. The floor is radar-dark, indicating a lack of coarse, reflective material. Exterior to the crater, the surface has a radar return similar to that of the surrounding plain.

3. Crater Circularities

Impact craters tend to be more circular in planimetric form than craters of other origins. Murray and Guest (1970) reviewed various methods to determine circularities and applied the results to the analysis of lunar craters. Oberbeck *et al.* (1972) modified this method and applied the technique to the analysis of martian craters. The technique may be important in the analysis of craters on radar images of Venus.

To assess the potential for deriving circularity values from radar images, circularity was determined for the 12 craters studied. Two sets of images were made for each crater, one set from the SIR-A data, the other set from conventional photography. Craters on both sets were enlarged to a uniform scale and a person unfamiliar with the craters determined circularity values, using the method of Oberbeck *et al.* (1972).

TABLE I

Characteristics of craters analyzed

Name	Type	Size (m)	Depth (m)	Circularity	
				Photo	SIR-A
MacDougal	Maar-collapse	1525 × 1738	131	1.09 (a)	1.03
Molina	Maar-collapse	450 × 500	30	1.11 (a)	1.15
Badillo	Maar-collapse	550 × 750	–	1.03 (a)	1.03
Crater Grande	Maar-collapse	976 × 1067	177	1.05 (a)	1.03
Kino	Maar-collapse	450 × 550	20	1.05 (b)	1.09
Celaya	Maar-collapse	800 × 900	80	1.07 (b)	1.04
Cerro Colorado	Maar-collapse	854 × 1067	10	1.04 (b)	1.05
Elegante	Maar-collapse	1311 × 1677	243	1.04 (a)	1.03
Moon	Maar-collapse	250 × 300	60	1.12 (b)	1.11
Cerro Volcan Quemado	Caldera-dome	2140 × 3400	75	1.18 (a)	1.16
Talemzane	Impact	1720 × 1750	70	1.07 (c)	1.04
Al Umchaimin	Impact (?)	3200 × 3200	35	1.01 (c)	1.04

(a) Conventional air photo.
(b) Skylab photo.
(c) Landsat photo.

Table I gives the results. In general, the radar values are within ~ 5% of the values derived from conventional photographs. The lower resolution of the radar images may cause the viewer to perceive a more regular outline to the crater. Moreover, the geometric projection of radar images is essentially rectilinear; hence, their 'true' planimetric form may be better represented. We conclude that the circularities of craters derived from radar images should be as valid as those derived from optical photographs.

4. Results and Discussion

Definitive identification of impact craters on Earth using remote sensing is, at best, difficult. As assessed from aerial photographs, fresh impact craters tend to: (1) be circular in plan form, (2) have rims which may be composed of overturned strata, (3) have rims raised above surrounding surfaces, (4) have floors lower than the surrounding surface, and (5) have fields of blocky ejecta and possibly secondary craters extending outward from the crater rim. Many of these criteria can be evaluated on radar images, although there are some important differences when compared with conventional images. On the one hand, radar images typically are of lower spatial resolution and features such as overturned strata in the crater rim may not be visible; on the other hand, blocky ejecta may be enhanced on radar images due to backscattering.

Of the various types of non-impact craters, maars are most likely to be confused with impact structures. However, in the Pinacate field all of the maar craters involved multiple eruptions which led to asymmetries in plan view and the irregular outlines are clearly visible on the radar images. Many of the maar craters at Pinacate have wall sections that are nearly vertical. Steep wall segments are visible as radar shadows on some of the craters, such as Crater Grande (Figure 4) and Elegante (Figure 8); however, the ability to detect steep walls on radar is a function of viewing geometry, incidence angle of the radar beam, and reflectivity of wall material.

In general, it does not appear possible to distinguish the elevations of the crater rim and floor in relation to the surrounding plain using SIR-A images, so these important relationships for the identification of impact craters could not be used. However, the Magellan radar data will be accompanied by altimetry data with a lateral resolution comparable to that of the radar ground resolution. This combination may be able to provide enough information about some relative crater elevations that some impact craters could be identified with certainty.

Many Pinacate craters display radar-dark floors with central bright spots; in one case, Moon crater, this bright spot results from the presence of a spatter cone that could be misinterpreted as a central peak typical of impact craters. In most cases, though, the dark floors correspond to alluvium and playa deposits and the central bright spots to vegetation. Although liquid water does not presently exist on the venusian surface, some models suggest the possibility of liquid water in the past (Donahue *et al.*, 1982), and craters may have received similar sediments. For

example, the floors of some venusian craters larger than 20 km are radar-dark in images produced by Earth-based radar (Cutts *et al.*, 1981). Vegetation is not considered to be a factor in radar images of Venus.

For interpretations of radar images of the Moon, Mars, and Venus, the distribution of surface facets has been modeled using combinations of Gaussian and exponential height and separation functions (Hagfors, 1964; Muhleman, 1964; and others). Using multiple-look-angle observations, an estimate of the RMS slope of the surfaces of these planets has been made (Hagfors *et al.*, 1965; Pettingill *et al.*, 1973; Downs *et al.*, 1975; Simpson *et al.*, 1978; and many others). SIR-A did not have a look angle which varies, so the angular distribution of reflected energy was not determined and a quantitative calculation of the surface slope and roughness could not be made. Magellan, however, will have a look angle which varies, and the potential will exist for calculating the slope and roughness of areas appearing in overlapping images; such data could help constrain the RMS estimates for Venus, and could contribute to quantitative analysis of rim roughness on certain craters.

As imaged by SIR-A, the rim crests and outer flanks of the impact structures and several of the volcanic craters are radar-bright as a result of blocks. The blocks range in size from ~ 30 cm to > 2 m across. In general, both block size and frequency decrease with radial distance from the rim. On radar images, the brightness also decreases in intensity from the rim crest outward. Some of the craters, however, have been weathered and eroded (e.g., Al Umchaimin), or mantled by younger deposits (e.g., Moon crater), and do not show this radar pattern. In other cases (e.g., Elegante), the flank is radar-mottled not from blocks, but from erosional gullies that serve as radar scatterers. Thus, it would be very difficult to distinguish impact craters from certain volcanic craters solely on patterns of radar brightness on crater flanks, especially if the surface had been weathered and eroded or partly mantled.

Although craters on Venus may not be gullied by water, wind erosion may play a similar role, producing bright radar returns. Moreover, mantling by aeolian, volcanic, or impact-generated deposits would tend to produce dark or diffuse areas on radar images. Blocky ejecta may not be as predominant on venusian impact rims as on Earth due to much higher temperatures at shallow depths (Anderson, 1981). Since Magellan's radar wavelength is approximately half that of SIR-A, a bright backscatter return would be produced by smaller blocks. Thus, because smaller blocks are distributed around the crater at a greater distance than larger blocks, a crater such as Al Umchaimin would probably appear on a Magellan radar image with a somewhat wider bright ring than on the SIR-A image.

Potential differences in venusian and terrestrial eruptive styles also must be taken into consideration when extrapolating terrestrial results to Venus. The high surface temperatures and pressures coupled with the lack of liquid water on Venus may imply that pyroclastic eruptions are rare and that maar craters may not exist (Garvin *et al.*, 1982; Head and Wilson, 1982).

In conclusion, radar images display some of the features commonly employed in the identification of impact craters, including circular planimetric form and blocky

ejecta on the crater flanks. However, these same features are also characteristic of some types of volcanic craters. Moreover, central volcanic cones may produce radar-bright zones which could be misinterpreted as central peaks of impact craters. We note that these factors must be taken into account in the analysis of craters on Venus using radar images, and that the geological setting of the craters in question may be as important as the morphology of the craters in determining their origin.

Acknowledgments

We thank the Planetary Geology Group at Arizona State University for field assistance during work in the Pinacate volcanic field and Raul Carrasco of Servicio Geologico de Bolivia (GEOBOL) for facilitating the work in the Altiplano. Edward Albin determined the crater circularities and reduced the related data. We also thank three anonymous reviewers for their invaluable suggestions and comments.

This work was partly supported by a contract from the Jet Propulsion Laboratory (No. 956428) and by a grant (NSG 7415) from the Office of Planetary Geology, National Aeronautics and Space Administration.

References

Ahlfeld, F. E.: 1972, *Geologia de Bolivia*, Los Amigos del Libro, La Paz, 190 pp.

Anderson, D. L.: 1981, *Geophys. Res. Letters* **8**, 309.

Arvidson, R. E. and Mutch, T. A.: 1974, *Geol. Soc. Am. Bull.* **85**, 99.

Basilevsky, A.: 1984, 'Impact Craters on Venus', paper presented at *Lunar Planet. Sci. 15th.*

Beckmann, P. and Spizzichino, A.: 1963, *The Scattering of Electromagnetic Waves from Rough Surfaces*, Pergamon, New York.

Brady, L. F.: 1954, 'The Crater of Talemzane in Algeria', *Sky and Telescope* **13**, 297.

Burns, B. A. and Campbell, D. B.: 1985, *J. Geophys. Res.* **90**, 3037.

Campbell, D. B. and Burns, B. A.: 1980, *J. Geophys. Res.* **85**, 8271.

Campbell, M. J. and Ulrichs, J.: 1969, *J. Geophys. Res.* **74**, 5867.

Cutts, J. A., Thompson, T. W., and Lewis, B. H.: 1981, *Icarus* **48**, 428.

Donahue, T. M., Hoffman, J. H., Hodges, R. R., Jr., and Watson, A. J.: 1982, *Science* **216**, 630.

Donnelly, M.: 1974, *Geology of the Sierra del Pinacate Volcanic Field, Northern Sonora, Mexico, and Southern Arizona, U.S.A.*, (Ph.D. dissert.), Stanford, Calif., Stanford Univ., 722 pp.

Downs, G. S., Reichley, P. E., and Green, R. R.: 1975, *Icarus* **26**, 273.

Elachi, C., Brown, W. E., Cimino, J. B., Dixon, T., Evans, D. L., Ford, J. P., Saunders, R. S., Breed, C., Masursky, H., McCauley, J. F., Schaber, G., Dellwig, L., England, A., MacDonald, H., Martin–Kaye, P., and Sabins, F.: 1982, *Science* **218**, 996.

Garvin, J. B., Head, J. W., and Wilson, L.: 1982, *Icarus* **52**, 365.

Greeley, R. and Gault, D. E.: 1979, *Proc. Lunar Planet. Sci. Conf. 10th*, pp. 2919–2933.

Gutmann, J. T.: 1972, *Eruptive History and Petrology of Crater Elegante, Sonora, Mexico*, (Ph.D. dissert.), Stanford, Calif., Stanford Univ., 235 pp.

Gutmann, J. T.: 1976, *Geol. Soc. Am./ Bull.* **87**, 1718.

Gutmann, J. T. and Sheridan, M. F.: 1978, in D. M. Burt and T. L. Pewe (eds.), *Guidebook to the Geology of Central Arizona*, Arizona Bur. Mines and Mineral Tech., Spec. Paper 2, pp. 47–59.

Hagfors, T.: 1964, *J. Geophys. Res.* **69**, 3779.

Hagfors, T., Brockelman, R. A., Danforth, H. H., Hanson, L. B., and Hyde, G. M.: 1965, *Science* **150**, 1153.

Hartmann, W. K., Strom, R. G., Weidenschilling, S. J., Blasius, K. R., Woronow, A., Dence, M. R., Grieve, R. A. F., Diaz, J., Chapman, C. R., Shoemaker, E. M., and Jones, K. L.: 1981, in *Basaltic Volcanism on the Terrestrial Planets*, Pergamon Press, New York, pp. 1049–1127.

Head, J. W., Peterfreund, A. R., and Garvin, J. B.: 1985, *J. Geophys. Res.* **90**, 6873.
Head, J. W. and Wilson, L.: 1982, *Lunar Planet. Sci.* **13**, 312.
Head, J. W. and Wilson, L.: 1985, 'Volcanic Processes and Landforms on Venus: Theory, Predictions, and Observations', *J. Geophys. Res.* (in press).
Hoekstra, P. and Delaney, A.: 1974, *J. Geophys. Res.* **78**, 1699.
Jahns, R. H.: 1959, *Ariz. Geol. Soc. Digest* **2**, 165.
Jahns, R. H. and Fielder, R. G.: 1952, *Engin. and Sci.* **15**, 13.
Karpoff, R.: 1954, *C.R. Congress Geol. Internat. Alger, 1952*, Sect. 13, Fas. 14, pp. 233–241.
Lambert, P., McHone, J. F., Dietz, R. S., and Houfani, M.: 1980, *Meteoritics* **15**, 157.
Lynch, D. J.: 1981, *Genesis and Geochronology of Alkaline Volcanism in the Pinacate Volcanic Field, Northwestern Sonora, Mexico*, unpubl. Ph.D. thesis, Univ. of Arizona, Tucson, 248 pp.
Masursky, H., Eliason, E., Ford, P. G., McGill, G. E., Pettengill, G. H., Schaber, G. G., and Schubert, G.: 1980, *J. Geophys. Res.* **85**, 8232.
Merriam, R. and Holwerda, J. G.: 1957, *Geographical J.* **123**, 231.
Moore, H. J., Boyce, J. M., Schaber, G. G., and Scott, D. H.: 1980, 'Lunar Remote Sensing and Measurements', U.S. Geological Survey Professional Paper 1046-B.
Muhleman, D. O.: 1964, *Astron. J.* **69**, 34.
Murray, J. B. and Guest, J. E.: 1970, *Modern Geology* **1**, 149.
Oberbeck, V. R., Aoyagi, M., and Murray, J. B.: 1972, *Modern Geology* **3**, 195.
Pettengill, G. H., Eliason, E., Ford, P. G., Loriot, G. B., Masursky, H., and McGill, G. E.: 1980, *J. Geophys. Res.* **85**, 8261.
Pettengill, G. H., Shapiro, I. I., and Rogers, A. E. E.: 1973, *Icarus* **18**, 22.
Schaber, G. G. and Boyce, J. M.: 1977, in D. J. Roddy, R. O. Pepin, and R. B. Merrill (eds.), *Impact and Explosion Cratering*, Pergamon Press, New York, pp. 603–612.
Settle, M. and Taranik, V. V.: 1982, *Science* **218**, 993.
Simpson, R. A., Tyler, G. L., and Campbell, D. B.: 1978, *Icarus* **36**, 153.
Tyler, G. L., Simpson, R. A., and Moore, H. J.: 1971, *J. Geophys. Res.* **76**, 2790.
Wood, C. A.: 1974, *Bull. Volcanol.* **38**, 149.